## **Inorganic Chemistry**

pubs.acs.org/IC Article

# Growth, Structure, and Optical Properties of a Nonlinear Optical Niobium Borate Crystal CsNbOB<sub>2</sub>O<sub>5</sub> with Distorted NbO<sub>5</sub> Square Pyramids

Juhe Liu, Ming-Hsien Lee, Chunxiao Li, Xianghe Meng,\* and Jiyong Yao\*



Cite This: Inorg. Chem. 2022, 61, 19302–19308

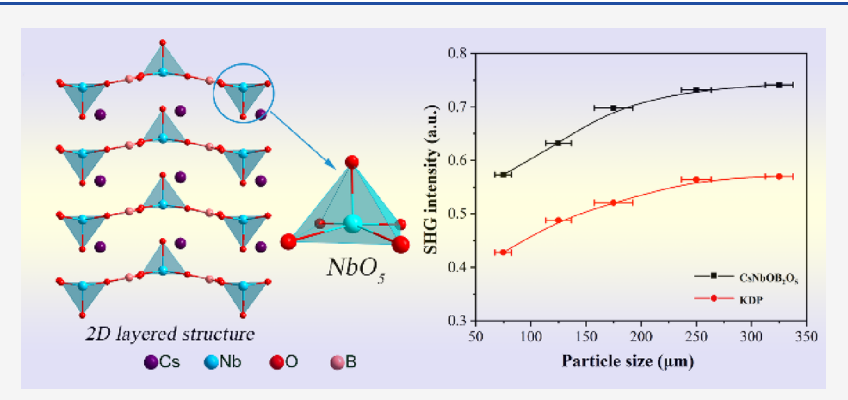


ACCESS

Metrics & More

Article Recommendations

s Supporting Information



**ABSTRACT:** In this paper, a revised structure determination of an already known compound CsNbOB<sub>2</sub>O<sub>5</sub> with new structural insights was performed and the detailed characterization of its optical properties was reported for the first time. CsNbOB<sub>2</sub>O<sub>5</sub> was synthesized by spontaneous crystallization. It crystallizes in the  $Pmn2_1$  space group, and the unit lattice parameters are a = 7.5220(7) Å, b = 3.9881(4) Å, c = 9.7167(9) Å, and Z = 2. In the structure of CsNbOB<sub>2</sub>O<sub>5</sub>, a [NbO<sub>5</sub>] square pyramid and [B<sub>2</sub>O<sub>5</sub>] unit are linked to constitute an infinitely extended two-dimensional  $_{\infty}^2$ [NbOB<sub>2</sub>O<sub>5</sub>] layer via sharing oxygen atoms. Between these two-dimensional layers, there are no covalent bonds perpendicular to their planes based on Mulliken bond order analysis. CsNbOB<sub>2</sub>O<sub>5</sub> has a wide band gap (4.52 eV) and a large second-harmonic-generation (SHG) response (1.2 × KDP) and demonstrates type-I phase-matchable behavior. First-principles simulations reveal that the birefringence is approximately 0.10. Moreover, SHG-weighted charge density analysis shows that the primary source of the nonlinearity of the title compound is the distorted NbO<sub>5</sub> square pyramids.

#### INTRODUCTION

Nonlinear optical (NLO) crystal materials are used in laser wavelength conversion technology. 1-9 Borates as important types of NLO crystals have always been a research hotspot for a long time. 10-15 The boron and oxygen atoms in borates can be three-coordinated and four-coordinated to form a (BO<sub>3</sub>)<sup>3-</sup> planar triangle and (BO<sub>4</sub>)<sup>5-</sup> tetrahedron, respectively; <sup>18</sup> especially, the conjugated  $\pi$ -orbitals and highly anisotropic electron distribution in the (BO<sub>3</sub>)<sup>3-</sup> group are very favorable for the enhancement of NLO performance and the generation of birefringence. 19,20 The large electronegativity difference between boron and oxygen atoms is beneficial to ultraviolet (UV) transmittance. If the hanging bond on the oxygen anion in the B-O group is eliminated, the UV cutoff edge of the compound will be further shortened, which is likely to make the compounds useful in the deep ultraviolet (DUV) region.<sup>21</sup> Through the long-term and unremitting efforts of researchers, many borates with excellent properties have been discovered, including  $\beta$ -BaB<sub>2</sub>O<sub>4</sub> (BBO), LiB<sub>3</sub>O<sub>5</sub> (LBO), and KBe<sub>2</sub>BO<sub>3</sub>F<sub>2</sub> (KBBF).<sup>24</sup> However, they still have some defects. For example, the applications of BBO and LBO in the DUV area are limited for their relatively narrow energy bandgaps and low birefringence values, respectively. Moreover, KBBF needs highly toxic BeO as the raw material, and it is hard to grow into large-high-quality single crystals due to its layered growth habit. Thus, exploring new NLO materials with excellent comprehensive performance is still a research hotspot in the field.

It is necessary to have a short absorption cutoff ( $\lambda_{\text{cutoff}}$ ) and a large nonlinear coefficient for NLO crystal materials applied in the UV and DUV areas. <sup>25,26</sup> Since alkali metals and alkaline

Received: August 30, 2022 Published: November 17, 2022





earth metals do not have d-d and f-f electron transitions,  $^{27-29}$  they are conducive to transmission in the UV or even DUV region. For a large nonlinear coefficient, it is a good idea to introduce metal cations with  $d^0$  electronic configuration ( $M^{n+} = Nb^{5+}$  and  $Ta^{5+}$ ) in borates.  $^{30-33}$   $Nb^{5+}$  and  $Ta^{5+}$  with  $d^0$  electron configuration are prone to Ginger-Taylor distortion,  $^{34-36}$  and when they combine with oxygen atoms, the asymmetric coordination environment can be formed to enhance the optical characteristics of the material greatly.

ANbOB<sub>2</sub>O<sub>5</sub> (A = K, Rb, and Cs)<sup>37-41</sup> as NLO materials have been proposed by Nicholls et al. However, for CsNbOB<sub>2</sub>O<sub>5</sub>, <sup>42</sup> only the crystal structure has been reported, and the NLO performance has not been characterized up to now. Although the three compounds have the same space group of Pmn21, there are still some differences in structural parameters and properties. For example, the unit cell volumes of KNbOB<sub>2</sub>O<sub>5</sub> and RbNbOB<sub>2</sub>O<sub>5</sub><sup>43</sup> are about 7 and 5 times that of CsNbOB<sub>2</sub>O<sub>5</sub>, which we synthesized, respectively. In addition, the unusual thing is that, in previous reports, KNbOB<sub>2</sub>O<sub>5</sub> cannot achieve phase matching (PM), but RbNbOB<sub>2</sub>O<sub>5</sub> can. We speculate that with the increase in the cation size, the birefringence 44-46 of the material increases so that RbNbOB<sub>2</sub>O<sub>5</sub> can achieve PM. Hence, we predict that CsNbOB<sub>2</sub>O<sub>5</sub> should also be able to achieve PM. To verify our conclusion, the polycrystalline powder synthesis and crystal growth for CsNbOB2O5 were immediately carried out, and the optical properties of CsNbOB2O5 were performed through experiments and theoretical calculation.

#### EXPERIMENTAL SECTION

**Reagents.** All reagents,  $Cs_2CO_3(99.8\%)$ ,  $Nb_2O_5(99.9\%)$ , and  $B_2O_3(99.9\%)$ , were purchased from Shanghai Aladdin Biochemistry Technology Co., Ltd.

**Single-Crystal Growth.** Single crystals of CsNbOB<sub>2</sub>O<sub>5</sub> were gained through a high-temperature solution technique (Figure S1). A platinum crucible was used to hold a mixture of Nb<sub>2</sub>O<sub>5</sub>, Cs<sub>2</sub>CO<sub>3</sub>, and B<sub>2</sub>O<sub>3</sub> in a 1:2.5:6.5 molar ratio. After grinding, the mixed raw materials was then put into a furnace and the temperature was increased from 30 to 900 °C and was maintained for 20 h. Subsequently, after 25 h, the temperature was reduced to 800 °C. Finally, it was allowed to naturally cool to 30 °C.

**Synthesis of Polycrystalline Powder.** Nb<sub>2</sub>O<sub>5</sub>, Cs<sub>2</sub>CO<sub>3</sub>, and B<sub>2</sub>O<sub>3</sub> were mixed according to a ratio of 0.92:0.98:2 for the synthesis of pure phase powder. If Nb<sub>2</sub>O<sub>5</sub>, Cs<sub>2</sub>CO<sub>3</sub>, and B<sub>2</sub>O<sub>3</sub> are reacted in a stoichiometric molar ratio of 1:1:2, the reaction product will contain impurities of Cs<sub>5</sub>Nb<sub>13</sub>O<sub>35</sub>, which is caused by the volatilization of raw materials (B<sub>2</sub>O<sub>3</sub> > Cs<sub>2</sub>CO<sub>3</sub> > Nb<sub>2</sub>O<sub>5</sub>) during the reaction. Therefore, it is a good method to obtain a pure phase by unevenly reducing the content of Nb<sub>2</sub>O<sub>5</sub> and Cs<sub>2</sub>CO<sub>3</sub>. The above sample was fully ground and put into a corundum crucible, calcined at 773 K for 10 h, ground again, and then heated to 1073 K for 1 day to obtain the target compound. The sample is pure based on the powder X-ray diffraction (PXRD). (Figure S2).

**Powder X-ray Diffraction (PXRD).** The PXRD data of the powder sample was obtained on a Bruker D8 Focus diffractometer equipped with Cu K $\alpha$  radiation ( $\lambda$  = 1.5418 Å) at room temperature. The test parameters are  $0.02^{\circ}$  scan step width, 0.1 s/step scan speed, and  $10-70^{\circ}$   $2\theta$  range.

**Single-Crystal Structure Determination.** The crystal structure was analyzed using a single-crystal X-ray diffractometer. Diffraction data for the target compound were gained on a Rigaku AFC10 diffraction instrument with the equipment for graphite monochromatic Mo K $\alpha$  ( $\lambda$  = 0.71073 Å) radiation under 296.15 K. Data collection and absorption correction were performed using the CrysAlispro program and the Multiscan method. The crystal structure for CsNbOB<sub>2</sub>O<sub>5</sub> was resolved directly with the ShelXT program,<sup>47</sup>

and the structure of the crystal was optimized with ShelXL $^{48}$  using full matrix least-squares minimization on  $F^2$ . The important structure parameter information for CsNbOB $_2O_5$  is presented in Table 1.

Table 1. Crystal Data and Structure Refinement for CsNbOB<sub>2</sub>O<sub>5</sub><sup>a</sup>

empirical formula	CsNbOB <sub>2</sub> O <sub>5</sub>
formula weight	343.44
crystal system	orthorhombic
space group	$Pmn2_1$
a (Å)	7.5220(7)
b (Å)	3.9881(4)
c (Å)	9.7167(9)
$\alpha$ (°), $\beta$ (°), and $\gamma$ (°)	90
volume (ų)	291.49(5)
Z	2
$\rho_{\rm calc}~({ m g/cm^3})$	3.913
$\mu  \left( \mathrm{mm}^{-1} \right)$	8.178
F(000)	308.0
radiation	Mo K $\alpha$ ( $\lambda$ = 0.71073)
2 heta range for data collection (°)	6.85 to 66.348
index ranges	$-11 \le h \le 11, -6 \le k \le 6, -14 \le l \le 13$
independent reflections	1093 [ $R_{\text{int}} = 0.0458, R_{\text{sigma}} = 0.0455$ ]
data/restraints/parameters	1093/1/53
goodness-of-fit on $F^2$	1.142
final R indexes $[I \ge 2\sigma(I)]$	$R_1 = 0.0282, wR_2 = 0.0635$
final R indexes [all data]	$R_1 = 0.0286, wR_2 = 0.0637$
${}^{a}R_{1} = \Sigma   F_{o}  -  F_{c}  /\Sigma  F_{o} $ and $F_{o}^{2} > 2\sigma(F_{o}^{2})$ .	$wR_2 = \left[\Sigma w (F_o^2 - F_c^2)^2 / \Sigma w F_o^4\right]^{1/2}$ for

UV–vis–NIR Diffuse Reflectance Spectrometry. The diffuse reflectance spectra of  $CsNbOB_2O_5$  in the 200–2000 nm region were obtained (Figure S3). The UV–vis–NIR spectrometer employed is a PerkinElmer Lambda 900 with an integrating sphere.

**SHG Tests.** The powder SHG effect of CsNbOB<sub>2</sub>O<sub>5</sub> was tested using Kurtz and Perry techniques. <sup>49</sup> The experiment was carried out using a 1064 nm Q-switched Nd:YAG laser. The polycrystalline powder of CsNbOB<sub>2</sub>O<sub>5</sub> was finely ground. Then, the following particle size ranges are selected: 50-100, 100-150, 150-200, 200-300, and  $300-350~\mu m$ . Crystalline KDP samples were milled in the same way as a comparison.

**Thermal Analysis.** The thermal properties for CsNbOB $_2$ O $_5$  were detected by differential scanning calorimetric (DSC) analysis and thermogravimetric analysis (TGA) with an NETZSCH STA 409C/CD thermal analyzer. The temperature was first raised to 1100 °C and then lowered to 30 °C under a N $_2$  atmosphere with the same heating/cooling rate of 10 °C/min.

**Computational Methods.** First-principles calculations of  $CsNbOB_2O_5$  were conducted through utilizing a CASTEP software package according to density functional theory (DFT).  $^{50-53}$  The PBE (Perdew, Burke, and Ernzerhof) functionals of generalized gradient approximation (GGA) were adopted to describe the exchange–correlation effect.  $^{54}$  The plane-wave energy cutoff and the tolerance for self-consistent field convergence are set to 750 eV and  $10^{-6}$  eV/atom, respectively. Its electronic band structure was calculated from the experimentally obtained crystal structure. Then, the principal-axis refractive indexes and SHG coefficient  $d_{ij}$  were calculated using a DFPT method  $^{55,56}$  recently implemented in CASTEP. In addition, to analyze the main sources of compound nonlinearity in real space, the SHG-weighted density  $^{57,58}$  analysis tool was used.

#### ■ RESULTS AND DISCUSSION

**Structure Description.** CsNbOB<sub>2</sub>O<sub>5</sub> crystallizes in the  $Pmn2_1$  space group with unit lattice parameters of a = 7.5220(7) Å, b = 3.9881(4) Å, c = 9.7167(9) Å, and Z = 2. In

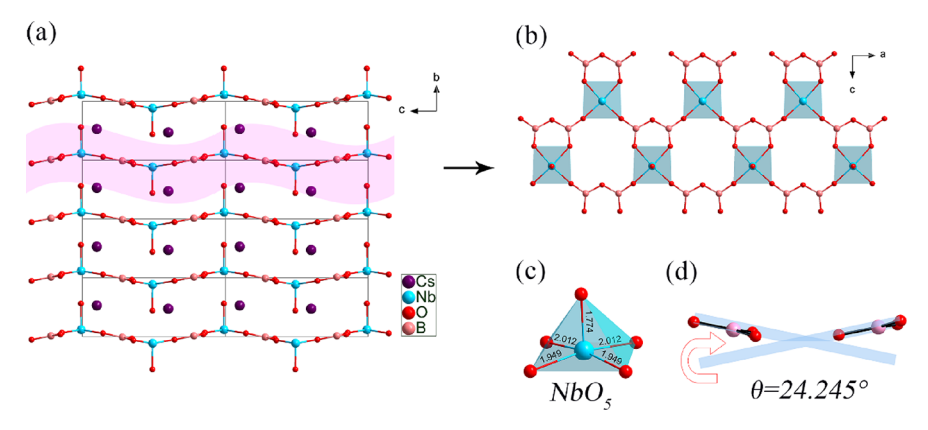


Figure 1. (a) Crystal structure of  $CsNbOB_2O_5$ . (b)  $[NbOB_2O_5]$  layer in  $CsNbOB_2O_5$ . (c)  $[NbO_5]$  polyhedron. (d) Included angle of the plane of two  $[B_2O_5]$  groups.

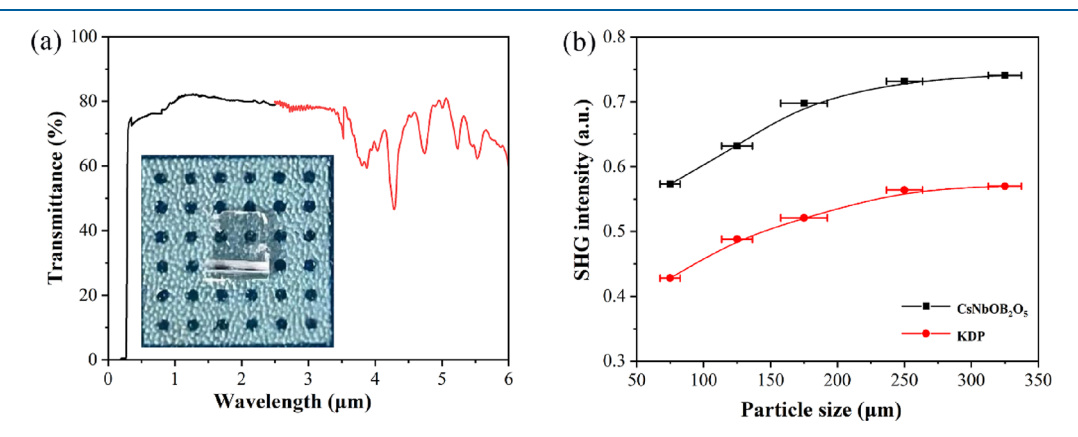


Figure 2. (a) Transmission spectrum of CsNbOB<sub>2</sub>O<sub>5</sub>. (b) Relationship between SHG intensity and particle size for CsNbOB<sub>2</sub>O<sub>5</sub>.

an article by Becker et al., 42 the Nb atom is connected with the surrounding six oxygen atoms to form a [NbO<sub>6</sub>] octahedron. The Nb atom is actually connected to the five oxygen atoms around it to form the [NbO<sub>5</sub>] unit through Mulliken bond order analysis. That means that the Nb cation should be pentacoordinated instead of hexacoordinated. Thus, the compound adopts a two-dimensional (2D) layered structure rather than a three-dimensional (3D) reticular structure described earlier. CsNbOB2O5 features a layered structure built from the [NbO<sub>5</sub>] square pyramids and [B<sub>2</sub>O<sub>5</sub>] groups, in which Cs+ species are filled to balance charge between layers (Figure 1a).  $[NbO_5]$  and  $[B_2O_5]$  groups are connected in the ac plane by oxygen atoms to constitute an unlimited twodimensional plane layer  $_{\infty}^{2}[NbOB_{2}O_{5}]$  (Figure 1b). For the [NbO<sub>5</sub>] square pyramid, the bond lengths between Nb atoms and the surrounding six oxygen atoms are not the same (Nb-O distances: 1.774-2.214 Å) (Figure 1c). In fact, no valence bond exists between the Nb atom and O atom with a distance of 2.214 Å, which we will explain below. The boron atom in CsNbOB<sub>2</sub>O<sub>5</sub> is tricoordinated, and the B-O length is 1.345-1.390 Å. The included angle of the plane where the  $[B_2O_5]$ units is located is 24.245° (Figure 1d). The oxygen atoms arranged around cesium atoms are irregular with the Cs-O length varying from 3.099 to 3.720 Å.

Thermal Stability. The DSC curve (Figure S4) shows an endothermic peak at 962 °C. This indicates that single crystals are melted around this temperature in the high-temperature resistance furnace. It can be seen that the melted and recrystallized product is free of the original phase, so the compound has an incongruent melting behavior (Figure S5).

The product of decomposition is  $Cs_4Nb_{11}O_{30}$ . Moreover, the weight of the compound decreased slightly from the 950 °C position in the TG curve, which may be caused by the volatilization of a small amount of borate.

Optical Properties. A regular shape CbNbOB<sub>2</sub>O<sub>5</sub> crystal (Figure S1) was obtained by spontaneous crystallization, and the transmittance was measured. We can see from the transmission spectrum (Figure 2a) that CsNbOB<sub>2</sub>O<sub>5</sub> has a high transmittance (≈80%) in the range from 300 to 3000 nm, and the UV cutoff edge is about 270 nm. The experimental band gap value was estimated to be 4.52 eV using a Tauc method. <sup>59</sup> Powder SHG characterization at discrete particle sizes using the Kurtz and Perry technique<sup>49</sup> was carried out to evaluate its NLO properties with KDP as a reference. According to the experimental findings, CsNbOB2O5's SHG intensity is almost 1.2 times that of KDP. Figure 2b depicts the variation trend of the SHG intensity of CsNbOB2O5 with crystallite size. With the increase in particle size, the nonlinear strength for CsNbOB<sub>2</sub>O<sub>5</sub> gradually increases and finally tends to saturation, which demonstrates the type-I PM performance of the crystal.

Previous experimental results show that  $KNbOB_2O_5$  fails to achieve PM, but  $RbNbOB_2O_5$  and  $CsNbOB_2O_5$  can. <sup>43</sup> We discovered that the crystal structure of  $ANbOB_2O_5$  (A = K, Rb, and Cs) is actually a layer-stacking type, which can be used to explain the difference in experimental results. The average layer-to-layer distances of  $KNbOB_2O_5$ ,  $RbNbOB_2O_5$ , and  $CsNbOB_2O_5$  are 3.895, 3.928, and 3.988 Å, respectively. As the cation radius increases, the layer-to-layer distance is stretched, causing the decrease in the index of refraction in

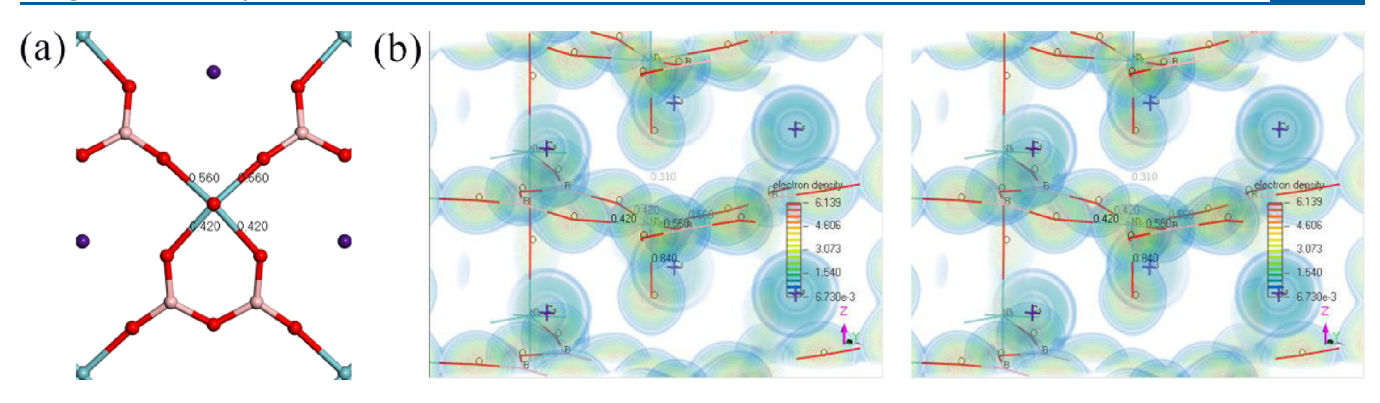


Figure 3. (a) Mulliken bond order of Nb–O bonds in the square planar unit. One can see the values of 0.56, 0.56, 0.42, 0.42, and the larger number is tilted toward the Z direction. (b) Cross-eye stereo pairs visualizing the total electron density and bond order index of Nb–O of a NbO<sub>S</sub> unit. The Nb–O terminal has a bond order index of 0.84, the largest among all Nb–O bonds. The bond order cross-connecting Nb and O between two NbO<sub>S</sub> units, however, has only an index value of 0.31, which is already as small as typical values between a cation and anion in a purely ionic crystal. Furthermore, from the volumetric total density plot, one can also that there is indeed no electron density between Nb and O from separate NbO<sub>S</sub> units to form a 3D linkage. Colors of elements: Nb (cyan), O (red), B (pink), and Cs (purple).

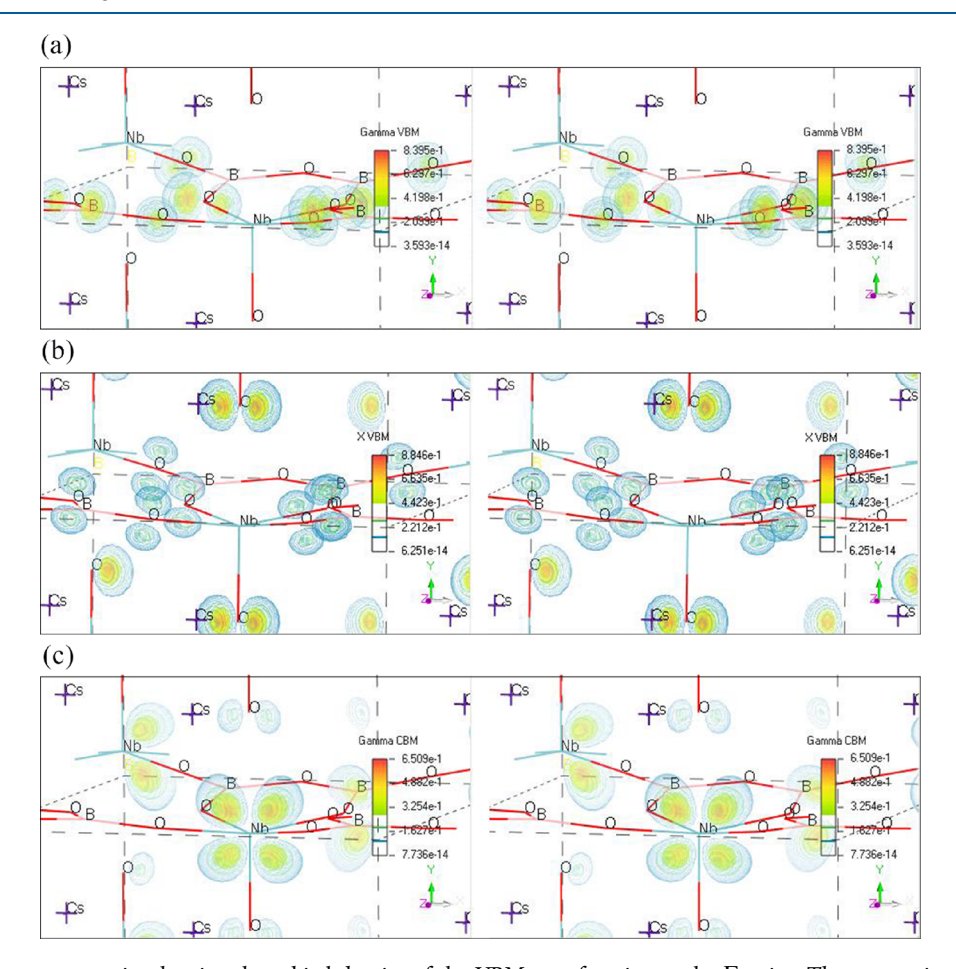


Figure 4. (a) Cross-eye stereo pairs showing the orbital density of the VBM wavefunction at the  $\Gamma$  point. The oxygen in the  $B_2O_5$ -NbO<sub>5</sub> plane contributes to the state. (b) Cross-eye stereo pairs showing the orbital density of the VBM wavefunction at the X point. The terminal oxygen in NbO<sub>5</sub> units contributes to the state. (c) Cross-eye stereo pairs showing the orbital density of the CBM wavefunction at the Γ point. The  $d_{xy}$  orbital of Nb has the dominant contribution.

the loosened direction (near vacuum) and ultimately resulting in an increase in the birefringence of the material. The birefringence values of KNbOB<sub>2</sub>O<sub>5</sub> and RbNbOB<sub>2</sub>O<sub>5</sub> are 0.032 and 0.05, respectively.<sup>63</sup> Cs ions and Rb ions have larger radii than K ions. CsNbOB<sub>2</sub>O<sub>5</sub> and RbNbOB<sub>2</sub>O<sub>5</sub> have larger birefringence than KNbOB<sub>2</sub>O<sub>5</sub>, so they can achieve PM under

1064 nm. In layered structures, controlling the birefringence by spacing cations is worthy of consideration.

Electronic Structure Calculations. First-principles simulations were performed to help comprehend how the structure and characteristics interact. Figure S6 illustrates that  $CsNbOB_2O_5$  shows an electronic transition from the X point to the  $\Gamma$  point with an indirect band gap of 3.54 eV. From the

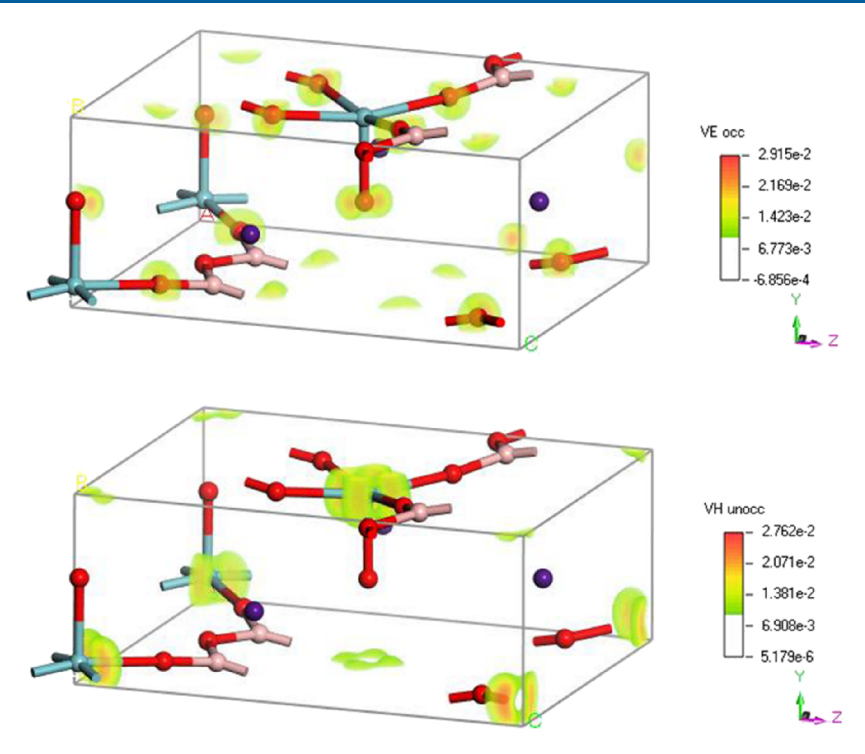


Figure 5. SHG-weighted density maps of occupied and unoccupied components in CsNbOB<sub>2</sub>O<sub>5</sub>.

total and partial density of states of  $CsNbOB_2O_5$  (Figure S6), we can draw the following conclusions: The top of the valence bands (VBs) mainly consists of the 2p orbitals of O, and the bottom of the conduction bands (CBs) mainly consists of the 4d orbital of Nb.

An interesting fact revealed from the result of calculated Mulliken bond population  $^{60-62}$  (bond order index) is that  $CsNbOB_2O_5$  is a true layer-stacking crystal. There exists a covalent bond network holding the extended 2D (X-Z plane)  $B_2O_5$ - $NbO_5$  sheets, but no covalent bond connecting these layers along the Y direction. Figure 3 shows the bond population (bond order index) and total electron density near square-pyramidal  $NbO_5$  units, and one can see that there is no effective covalent bond between Nb from one  $NbO_5$  unit to bond to the tip (terminal) oxygen of the next layer  $NbO_5$ 

From the calculated band structure (Figure S6), one can see that the crystal has an indirect gap, from the X point to  $\Gamma$  point, although the energy required for the direct  $\Gamma$  to  $\Gamma$  transition is only slightly larger. In Figure 4, we show the orbital density of the specific one-particle orbitals from those k-points. The main difference between the  $\Gamma$  and X wavefunctions of VBM is the source of oxygen; in  $\Gamma$ , it mainly consists of planar oxygen, whereas in X, it comes almost entirely from terminal oxygen.

SHG-density<sup>57,58</sup> analysis shows that the NbO<sub>5</sub> unit is the main contributor of  $d_{33}$  from this crystal, as can be seen in Figure 5. For the occupied electronic subsystem, terminal oxygen has a slightly larger contribution than those in-plane (bridging) oxygens, but there is more bridging oxygen in the network. As for unoccupied orbitals, the  $d_{x-z}^{2}$ -orbital of Nb plays the major role.

It is well known that structural asymmetry causes SHG. In our computational analysis, the NbO<sub>5</sub> square pyramids distorted along the Z direction line up in space to deliver a large  $d_{33} = -0.10033$  pm/V. The 2D layered stacking along the

Y direction makes  $n_y$  the smallest compared to  $n_x$  and  $n_z$ , which results in the large birefringence  $(\Delta n)$ . The same as the case of  $d_{ij}$  here, the calculated birefringence using the recently implemented DFPT<sup>55,56</sup> method is roughly 0.1 in a wide range of wavelengths. These reasonably large  $d_{ij}$  and  $\Delta n$  predicted from our first-principles calculations is consistent with the type-I PM observed experimentally.

#### CONCLUSIONS

In general, niobium borate CsNbOB $_2$ O $_5$  with a distinctive two-dimensional layered structure was obtained by spontaneous crystallization. It has a large second-order NLO response (1.2 × KDP), wide band gap (~4.52 eV), and short UV cutoff edge (~270 nm). First-principles simulations reveal that the birefringence is approximately 0.10, and the [NbO $_5$ ] square pyramids are the primary source of the SHG response according to the SHG-density map. This study provides not only potential NLO crystals in the UV region for now but also some insights for discovering new NLO materials for follow-up research studies.

### ASSOCIATED CONTENT

#### Supporting Information

The Supporting Information is available free of charge at https://pubs.acs.org/doi/10.1021/acs.inorgchem.2c03083.

Picture of crystals, UV-vis-NIR spectrum, experimental and simulated PXRD patterns, TG-DSC curves, PXRD patterns before and after melting, calculated electronic band structure and density of states for CsNbOB<sub>2</sub>O<sub>5</sub>, and crystallographic data (PDF)

#### **Accession Codes**

CCDC 2205589 contains the supplementary crystallographic data for this paper. These data can be obtained free of charge via www.ccdc.cam.ac.uk/data\_request/cif, or by emailing data request@ccdc.cam.ac.uk, or by contacting The Cam-

bridge Crystallographic Data Centre, 12 Union Road, Cambridge CB2 1EZ, UK; fax: +44 1223 336033.

#### AUTHOR INFORMATION

#### **Corresponding Authors**

Xianghe Meng — Beijing Center for Crystal Research and Development, Key Lab of Functional Crystals and Laser Technology, Technical Institute of Physics and Chemistry, Chinese Academy of Sciences, Beijing 100190, P. R. China; Center of Materials Science and Optoelectronics Engineering, University of Chinese Academy of Sciences, Beijing 100049, P. R. China; Email: mengxianghe@mail.ipc.ac.cn

Jiyong Yao — Beijing Center for Crystal Research and Development, Key Lab of Functional Crystals and Laser Technology, Technical Institute of Physics and Chemistry, Chinese Academy of Sciences, Beijing 100190, P. R. China; Center of Materials Science and Optoelectronics Engineering, University of Chinese Academy of Sciences, Beijing 100049, P. R. China; ⊚ orcid.org/0000-0002-4802-5093; Email: jyao@mail.ipc.ac.cn

#### Author

Juhe Liu — Beijing Center for Crystal Research and Development, Key Lab of Functional Crystals and Laser Technology, Technical Institute of Physics and Chemistry, Chinese Academy of Sciences, Beijing 100190, P. R. China; Center of Materials Science and Optoelectronics Engineering, University of Chinese Academy of Sciences, Beijing 100049, P. R. China; University of Chinese Academy of Sciences, Beijing 100049, P. R. China

Ming-Hsien Lee – Department of Physics, Tamkang University, New Taipei 25137, Taiwan; ⊚ orcid.org/0000-0003-3956-181X

Chunxiao Li — Beijing Center for Crystal Research and Development, Key Lab of Functional Crystals and Laser Technology, Technical Institute of Physics and Chemistry, Chinese Academy of Sciences, Beijing 100190, P. R. China; Center of Materials Science and Optoelectronics Engineering, University of Chinese Academy of Sciences, Beijing 100049, P. R. China; University of Chinese Academy of Sciences, Beijing 100049, P. R. China

Complete contact information is available at: https://pubs.acs.org/10.1021/acs.inorgchem.2c03083

#### **Author Contributions**

J.L.: experimental testing, preparation of the original draft. M.-H.L.: theoretical analysis. C.L.: data analysis. X.M.: structure analysis and manuscript revision. J.Y.: supervision.

#### Notes

The authors declare no competing financial interest.

#### ACKNOWLEDGMENTS

This work was supported by the National Natural Science Foundation of China (nos. 22175190 and 51890862).

#### REFERENCES

- (1) Tran, T. T.; Yu, H.; Rondinelli, J. M.; Poeppelmeier, K. R.; Halasyamani, P. S. Deep Ultraviolet Nonlinear Optical Materials. *Chem. Mater.* **2016**, 28, 5238–5258.
- (2) Fu, Q.; Wu, Y.; Liang, S.; Shardlow, P. C.; Shepherd, D. P.; Alam, S.-u.; Xu, L.; Richardson, D. J. Controllable duration and repetition-rate picosecond pulses from a high-average-power OP-GaAs OPO. *Opt. Lett.* **2020**, *28*, 32540–32548.

- (3) Yao, J.; Mei, D.; Bai, L.; Lin, Z.; Yin, W.; Fu, P.; Wu, Y. BaGa<sub>4</sub>Se<sub>7</sub>: a new congruent-melting IR nonlinear optical material. *Inorg. Chem.* **2010**, 49, 9212–9216.
- (4) Murray, R. T.; Chandran, A. M.; Battle, R. A.; Runcorn, T. H.; Schunemann, P. G.; Zawilski, K. T.; Guha, S.; Taylor, J. R. Seeded optical parametric generation in CdSiP<sub>2</sub> pumped by a Raman fiber amplifier at 1.24  $\mu$ m. *Opt. Lett.* **2021**, *46*, 2039–2042.
- (5) Deng, Y.; Huang, L.; Dong, X.; Wang, L.; Ok, K. M.; Zeng, H.; Lin, Z.; Zou, G. K<sub>2</sub>Sb(P<sub>2</sub>O<sub>7</sub>)F: Cairo Pentagonal Layer with Bifunctional Genes Reveal Optical Performance. *Angew. Chem., Int. Ed.* **2020**, *59*, 21151–21156.
- (6) Fang, Q.; Yu, H.; Zhang, H.; Zhang, G.; Wang, J.; Wu, Y. Output power enhancement of a self-frequency-doubled laser by selective excitation of inequivalent active centers in  $La_2CaB_{10}O_{19}$  (Nd:LCB) crystal. *Opt. Lett.* **2017**, *42*, 4861–4864.
- (7) Guo, S.-P.; Cheng, X.; Sun, Z.-D.; Chi, Y.; Liu, B.-W.; Jiang, X.-M.; Li, S.-F.; Xue, H.-G.; Deng, S.; Duppel, V.; Köhler, J.; Guo, G.-C. Large Second Harmonic Generation (SHG) Effect and High Laser-Induced Damage Threshold (LIDT) Observed Coexisting in Gallium Selenide. *Angew. Chem., Int. Ed.* **2019**, *58*, 8087–8091.
- (8) Li, X.-H.; Shi, Z.-H.; Yang, M.; Liu, W.; Guo, S.-P. Sn<sub>7</sub>Br<sub>10</sub>S<sub>2</sub>: The First Ternary Halogen-Rich Chalcohalide Exhibiting a Chiral Structure and Pronounced Nonlinear Optical Properties. *Angew. Chem., Int. Ed.* **2022**, *61*, No. e202115871.
- (9) Lu, W.; Gao, Z.; Liu, X.; Tian, X.; Wu, Q.; Li, C.; Sun, Y.; Liu, Y.; Tao, X. Rational Design of a LiNbO<sub>3</sub>-like Nonlinear Optical Crystal, Li<sub>2</sub>ZrTeO<sub>6</sub>, with High Laser-Damage Threshold and Wide Mid-IR Transparency Window. *J. Am. Chem. Soc.* **2018**, *140*, 13089–13096.
- (10) Yang, G.; Gong, P.; Lin, Z.; Ye, N. AZn<sub>2</sub>BO<sub>3</sub>X<sub>2</sub>(A = K, Rb, NH<sub>4</sub>; X = Cl, Br): New Members of KBBF Family Exhibiting Large SHG Response and the Enhancement of Layer Interaction by Modified Structures. *Chem. Mater.* **2016**, 28, 9122–9131.
- (11) Jin, C.; Li, F.; Cheng, B.; Qiu, H.; Yang, Z.; Pan, S.; Mutailipu, M. Double-Modification Oriented Design of a Deep-UV Birefringent Crystal Functionalized by  $[B_{12}O_{16}F_4(OH)_4]$  Clusters. *Angew. Chem., Int. Ed.* **2022**, *61*, No. e202203984.
- (12) Liu, W.; Liu, X.; Meng, X.; Li, C.; Sun, M.; Lin, Z.; Yao, J. Two non-centrosymmetric scandium borate nonlinear optical crystals containing the B5O10 anion group. *J. Alloys Compd.* **2022**, 902, No. 163832.
- (13) Chen, Y.; Liu, W.; Feng, J.; Guo, R.; Fan, F.; Shen, J.; Zhang, G.; Tu, H. Magnetocaloric Effect in  $LiLn_6O_5$  (BO $_3$ )  $_3$  (Ln= Gd, Tb, Dy, and Ho). Cryogenics **2022**, No. 103476.
- (14) Li, Y.; Zhou, Z.; Zhao, S.; Liang, F.; Ding, Q.; Sun, J.; Lin, Z.; Hong, M.; Luo, J. A Deep-UV Nonlinear Optical Borosulfate with Incommensurate Modulations. *Angew. Chem., Int. Ed.* **2021**, *60*, 11457–11463.
- (15) Xie, Z.; Wang, Y.; Cheng, S.; Han, G.; Yang, Z.; Pan, S. Synthesis, characterization, and theoretical analysis of three new nonlinear optical materials K<sub>7</sub>MRE<sub>2</sub>B<sub>15</sub>O<sub>30</sub> (M= Ca and Ba, RE= La and Bi). Sci. China Mater. **2019**, *62*, 1151–1161.
- (16) Chen, C.; Wu, Y.; Li, R. The anionic group theory of the non-linear optical effect and its applications in the development of new high-quality NLO crystals in the borate series. *Int. Rev. Phys. Chem.* **1989**, *8*, 65–91.
- (17) Mutailipu, M.; Xie, Z.; Su, X.; Zhang, M.; Wang, Y.; Yang, Z.; Janjua, M. R. S. A.; Pan, S. Chemical Cosubstitution-Oriented Design of Rare-Earth Borates as Potential Ultraviolet Nonlinear Optical Materials. *J. Am. Chem. Soc.* **2017**, *139*, 18397–18405.
- (18) Liang, F.; Kang, L.; Gong, P.; Lin, Z.; Wu, Y. Rational Design of Deep-Ultraviolet Nonlinear Optical Materials in Fluorooxoborates: Toward Optimal Planar Configuration. *Chem. Mater.* **2017**, 29, 7098—7102.
- (19) Song, Y.; Luo, M.; Liang, F.; Ye, N.; Lin, Z. The second-harmonic generation intensification derived from localization conjugated π-orbitals in O<sub>22</sub>. Chem. Commun. 2018, 54, 1445–1448.
- (20) Song, J.-L.; Hu, C.-L.; Xu, X.; Kong, F.; Mao, J.-G. A Facile Synthetic Route to a New SHG Material with Two Types of Parallel

- $\pi$ -Conjugated Planar Triangular Units. Angew. Chem., Int. Ed. **2015**, 54, 3679–3682.
- (21) Chen, C.; Ye, N.; Lin, J.; Jiang, J.; Zeng, W.; Wu, B. Computer-Assisted Search for Nonlinear Optical Crystals. *Adv. Mater.* **1999**, *11*, 1071–1078.
- (22) Chen, C.; Wu, B.; Jiang, A.; You, G. A New-Type Ultraviolet SHG Crystal —— $\beta$ -BaB<sub>2</sub>O<sub>4</sub>. Sci. Sin, Ser. B **1985**, 28, 235–243.
- (23) Chen, C.; Wu, Y.; Jiang, A.; Wu, B.; You, G.; Li, R.; Lin, S. New Nonlinear-Optical Crystal: LIB<sub>3</sub>O<sub>5</sub>. *J.Opt. Soc. Am. B.* **1989**, *6*, 616–621.
- (24) Xia, Y.; Chen, C.; Tang, D.; Wu, B. New Nonlinear-Optical Crystals for UV and VUV Harmonic Generation. *Adv. Mater.* **1995**, *7*, 79–81.
- (25) Zou, G.; Ok, K. M. Novel ultraviolet (UV) nonlinear optical (NLO) materials discovered by chemical substitution-oriented design. *Chem. Sci.* **2020**, *11*, 5404–5409.
- (26) Lee, H.; Ok, K. M.  $Na_2Mg_{1-x}Zn_xSiO_4$  (0  $\leq x \leq 1$ ): Noncentrosymmetric Sodium Metal Silicate Solid Solutions with Ultraviolet Nonlinear Optical Properties. *Bull. Korean Chem. Soc.* **2020**, *41*, 139–142.
- (27) Dong, X.; Jing, Q.; Shi, Y.; Yang, Z.; Pan, S.; Poeppelmeier, K. R.; Young, J.; Rondinelli, J. M. Pb<sub>2</sub>Ba<sub>3</sub>(BO<sub>3</sub>)<sub>3</sub>Cl: A Material with Large SHG Enhancement Activated by Pb-Chelated BO<sub>3</sub> Groups. *J. Am. Chem. Soc.* **2015**, *137*, 9417–9422.
- (28) Wei, Q.; Cheng, J.-W.; He, C.; Yang, G.-Y. An Acentric Calcium Borate  $Ca_2[B_5O_9]\cdot (OH)\cdot H_2O$ : Synthesis, Structure, and Nonliner Optical Property. *Inorg. Chem.* **2014**, *53*, 11757–11763.
- (29) Zhang, H.; Zhang, M.; Pan, S.; Yang, Z.; Wang, Z.; Bian, Q.; Hou, X.; Yu, H.; Zhang, F.; Wu, K.; Yang, F.; Peng, Q.; Xu, Z.; Chang, K. B.; Poeppelmeier, K. R. Na<sub>3</sub>Ba<sub>2</sub>(B<sub>3</sub>O<sub>6</sub>)<sub>2</sub>F: Next Generation of Deep-Ultraviolet Birefringent Materials. *Cryst. Growth Des.* **2015**, *15*, 523–529.
- (30) Halasyamani, P. S. Asymmetric Cation Coordination in Oxide Materials: Influence of Lone-Pair Cations on the Intra-octahedral Distortion in d<sup>0</sup> Transition Metals. *Chem. Mater.* **2004**, *16*, 3586–3592.
- (31) Ok, K. M.; Halasyamani, P. S.; Casanova, D.; Llunell, M.; Alemany, P.; Alvarez, S. Distortions in Octahedrally Coordinated d<sup>0</sup> Transition Metal Oxides: A Continuous Symmetry Measures Approach. *Chem. Mater.* **2006**, *18*, 3176–3183.
- (32) Kunz, M.; Brown, I. D. Out-of-Center Distortions around Octahedrally Coordinated d0 Transition Metals. *J. Solid State Chem.* **1995**, *115*, 395–406.
- (33) Huang, J.; Guo, S.; Zhang, Z.; Yang, Z.; Pan, S. Designing excellent mid-infrared nonlinear optical materials with fluorooxofunctional group of d<sup>0</sup> transition metal oxyfluorides. *Sci. China Mater.* **2019**, *62*, 1798–1806.
- (34) Bersuker, I. B. Modern Aspects of the Jahn-Teller Effect Theory and Applications To Molecular Problems. *Chem. Rev.* **2001**, *101*, 1067–1114.
- (35) Bersuker, I. *The Jahn-Teller Effect*; Cambridge University Press: Cambridge, 2009.
- (36) Jahn, H. A.; Teller, E. Stability of polyatomic molecules in degenerate electronic states I—Orbital degeneracy. *Proc. R. Soc. London, Ser. A* 1937, 161, 220–235.
- (37) Akella, A.; Keszler, D. A. Crystal Chemistry of Noncentrosymmetric Alkali-Metal Nb and Ta Oxide Pyroborates. *J. Solid State Chem.* **1995**, *120*, 74–79.
- (38) Baucher, A.; Gasperin, M. Sur une nouvelle famille d'oxydes multiples a base de bore: MIM'VB $_2$ O $_6$  (M=Tl,Rb; M'=Nb,Ta). *Mater. Res. Bull.* **1975**, 10, 469–472.
- (39) Nicholls, J. F. H.; Henderson, B.; Chai, B. H. T. Structure and optical properties of the RbNbB<sub>2</sub>O<sub>6</sub> family of mixed borates. *Opt. Mater.* **1997**, *8*, 215–226.
- (40) Baucher, A.; Gasperin, M.; Cervelle, B. RbNbB<sub>2</sub>O<sub>6</sub>: structure de la maille multiple et propriétés optiques. *Acta Crystallogr., Sect. B: Struct. Crystallogr. Cryst. Chem.* **1976**, 32, 2211–2215.
- (41) Schmid, S.; Withers, R. L.; Corker, D.; Baules, P. Towards a unified description of the AMOB<sub>2</sub>O<sub>5</sub> (A=K, Rb, Cs, Tl; M=Nb, Ta)

- family of compounds. Acta Crystallogr., Sect. B: Struct. Sci. 2000, 56, 558-564.
- (42) Becker, P.; Bohatý, L.; Fröhlich, R. CsNbOB<sub>2</sub>O<sub>5</sub>: the Basic Structure Type of the Borates AMOB<sub>2</sub>O<sub>5</sub> (A = K, Rb, Cs, Tl; M = Nb, Ta). Acta Crystallogr., Sect. C: Cryst. Struct. Commun. **1995**, 51, 1721–1723.
- (43) Nicholls, J. F. H.; Chai, B. H.-T.; Corker, D. L.; Calabrese, J. C.; Henderson, B. KNB (KNbB<sub>2</sub>O<sub>6</sub>) and its isomorphs: a new family of nonlinear optical materials. In *Growth, Characterization, and Applications of Laser Host and Nonlinear Crystals II*; SPIE, 1863, (21 July 1993). DOI: 10.1117/12.149261.
- (44) Liu, Y.; Liu, Y.; Lin, Z.; Li, Y.; Ding, Q.; Chen, X.; Li, L.; Zhao, S.; Hong, M.; Luo, J. Nonpolar Na<sub>10</sub>Cd(NO<sub>3</sub>)<sub>4</sub>(SO<sub>3</sub>S)<sub>4</sub> Exhibits a Large Second-Harmonic Generation. *CCS Chem.* **2021**, *4*, 526–531.
- (45) Li, Y.; Yin, C.; Yang, X.; Kuang, X.; Chen, J.; He, L.; Ding, Q.; Zhao, S.; Hong, M.; Luo, J. A Nonlinear Optical Switchable Sulfate of Ultrawide Bandgap. *CCS Chem.* **2021**, *3*, 2298–2306.
- (46) Li, Y.; Luo, J.; Ji, X.; Zhao, S. A Short-wave UV Nonlinear Optical Sulfate of High Thermal Stability. *Chin. J. Struct. Chem.* **2020**, 39, 485–402
- (47) Sheldrick, G. M. SHELXT Integrated space-group and crystal-structure determination. *Acta Crystallogr., Sect. A: Found. Adv.* **2015**, 71, 3–8.
- (48) Sheldrick, G. M. Crystal structure refinement with SHELXL. (2053–2296 (Electronic)).
- (49) Kurtz, S. K.; Perry, T. T. A powder technique for the evaluation of nonlinear optical materials. *J. Appl. Phys.* **1968**, *39*, 3798–3813.
- (50) Clark, S. J.; Segall, M. D.; Pickard, C. J.; Hasnip, P. J.; Probert, M. I. J.; Refson, K.; Payne, M. C. First principles methods using CASTEP. Z. Kristallogr. Cryst. Mater. 2005, 220, 567–570.
- (51) Hohenberg, P.; Kohn, W. Inhomogeneous Electron Gas. *Phys. Rev.* **1964**, *136*, B864–B871.
- (52) Kohn, W.; Sham, L. J. Self-Consistent Equations Including Exchange and Correlation Effects. *Phys. Rev.* **1965**, *140*, A1133–A1138.
- (53) Payne, M. C.; Teter, M. P.; Allan, D. C.; Arias, T. A.; Joannopoulos, J. D. Iterative minimization techniques for ab initio total-energy calculations: molecular dynamics and conjugate gradients. *Rev. Mod. Phys.* **1992**, *64*, 1045–1097.
- (54) Perdew, J. P.; Burke, K.; Ernzerhof, M. Generalized Gradient Approximation Made Simple. *Phys. Rev. Lett.* **1996**, *77*, 3865–3868.
- (55) Refson, K.; Tulip, P. R.; Clark, S. J. Variational density-functional perturbation theory for dielectrics and lattice dynamics. *Phys. Rev. B* **2006**, *73*, No. 155114.
- (56) Miwa, K. Prediction of Raman spectra with ultrasoft pseudopotentials. *Phys. Rev. B* **2011**, *84*, No. 094304.
- (57) Lo, C.-H. Master degree thesis (Supervised by Lee, M.-H.), Taking University, 2005, p29.
- (58) Lee, M.-H.; Yang, C.-H.; Jan, J.-H. Band-resolved analysis of nonlinear optical properties of crystalline and molecular materials. *Phys. Rev. B* **2004**, *70*, No. 235110.
- (59) Nowak, M.; Kauch, B.; Szperlich, P. Determination of energy band gap of nanocrystalline SbSI using diffuse reflectance spectroscopy. *Rev. Sci. Instrum.* **2009**, *80*, No. 046107.
- (60) Mulliken, R. S. Electronic Population Analysis on LCAO–MO Molecular Wave Functions. I. J. Chem. Phys. 1955, 23, 1833–1840.
- (61) Segall, M. D.; Pickard, C. J.; Shah, R.; Payne, M. C. Population analysis in plane wave electronic structure calculations. *Mol. Phys.* **1996**, *89*, 571–577.
- (62) Segall, M. D.; Shah, R.; Pickard, C. J.; Payne, M. C. Population analysis of plane-wave electronic structure calculations of bulk materials. *Phys. Rev. B* **1996**, *54*, 16317–16320.
- (63) Nicholls, J. F. H.; Henderson, B.; Chai, B. H. T. The nonlinear optical properties of the  $XYB_2O_6$  family of compounds. *Opt. Mater.* **2001**, *16*, 453–462.